Biosensors and Bioelectronics 26 (2011) 2953–2959

Contents lists available at ScienceDirect

Biosensors and Bioelectronics

journal homepage: www.elsevier.com/locate/bios

Three-step electrodeposition synthesis of self-doped polyaniline nanofiber-supported flower-like Au microspheres for high-performance biosensing of DNA hybridization recognition

Xinxing Wang[a,b,1], Tao Yang[a,1], Xiao Li[a], Kui Jiao[a,*]

[a] State Key Laboratory Base of Eco-chemical Engineering, College of Chemistry and Molecular Engineering, Qingdao University of Science and Technology, Qingdao 266042, China
[b] Department of Food Engineering and Nutritional, Yellow Sea Fisheries Research Institute, Qingdao 266071, China

ARTICLE INFO

Article history:
Received 27 August 2010
Received in revised form 7 November 2010
Accepted 27 November 2010
Available online 4 December 2010

Keywords:
Three-step electrodeposition
Au microsphere
Self-doped polyaniline nanofiber
DNA hybridization recognition
Electrochemical impedance spectroscopy

ABSTRACT

A three-step electrodeposition method has been successfully adopted to fabricate morphology-controlled novel Au microspheres on self-doped polyaniline nanofibers (nanoSPAN) modified glassy carbon electrode. The deposition conditions, such as $HAuCl_4$ concentration and deposition step, have significant influences on the morphologies and electrochemical properties of the resulted Au microspheres. Well hierarchical and homogeneously dispersed flower-like Au microspheres (HHFAu) were obtained under optimal conditions by the three-step electrodeposition strategy in 5.0 mM $HAuCl_4$ solution. HHFAu possess large surface area, excellent electron transfer ability and good biocompatibility. The DNA probe could be effectively attached to HHFAu and thus a high-performance DNA biosensor was constructed by using electrochemical impedance spectroscopy as detection method. A gene fragment of the cauliflower mosaic virus 35S gene, which is related to one of the screening genes for the transgenically modified plants, has been satisfactorily detected. The linear range was from 1.0×10^{-13} M to 1.0×10^{-6} M and the detection limit was 1.9×10^{-14} M. This HHFAu/nanoSPAN-based impedance biosensing platform holds great promise for the detection of other biological and chemical molecules.

1. Introduction

Composites based on conducting polymers and metal micro-/nanostructures have attracted considerable attention recently owing to their great academic and industrial interests (Fu et al., 2009; Pringle et al., 2008; Singh et al., 2008). The composites integrate the advantages of the individuals, and display synergistic effects. Therefore, the conductivity and biocompatibility of the composites are obviously improved. The improved characteristics originate from the strong electronic interactions between the metal micro-/nanostructure and the conducting polymer, where the conducting polymer virtually acts as a matrix to support and disperse the metal micro-/nanostructure (Granot et al., 2005; Hatchett and Josowicz, 2008; Crespilhoa et al., 2009; Njagi and Andreescu, 2007).

Au micro-/nanostructure, as one of the most important metal functional materials, has received increasing interests due to its specific performances of electrical conductivity and biocompatibility (Zhao et al., 2008). It is known that its unique properties are related to its "size effect" (Lee et al., 2004; Subramanian et al., 2004). A large number of composites of Au micro-/nanostructures connected with conducting polymers have been prepared (Njagi and Andreescu, 2007; Rahman et al., 2008). Among these conducting polymers, polyaniline (PAN) is widely adopted due to its good electrical conductivity. Furthermore, the abundant amine and imine groups on the PAN backbone are propitious to adsorb metal ions (Gao et al., 2008; Guo et al., 2009). However, PAN is limited redox active only under acidic conditions, normally at pH < 4 (Tarver et al., 2009). This drawback greatly restricts its applicability in bioelectrochemistry, which normally requires a neutral pH environment. Copolymerization of aniline and *m*-aminobenzenesulfonic acid in aqueous solution, forming a kind of "so-called" self-doped polyaniline (SPAN, Zhang et al., 2009a), could overcome this drawback successfully. This SPAN is electroactive in neutral pH range through the introduction of $-SO_3H$ groups on its polymer backbone (Zhang et al., 2009c; Hu et al., 2010). In addition, SPAN has better hydrophilicity than PAN due to doping of the hydrophilic groups, which is propitious to adsorb metal ions and biomolecules. At the same time, the sulfonic acid groups and the imine units in SPAN have been used as nuclei for the reduction of some metal ions (Reddy et al., 2006). Self-doped polyaniline nanofibers (nanoSPAN) not only retain the electrochemical prop-

* Corresponding author. Tel.: +86 532 84022665; fax: +86 532 84023927.
E-mail address: kjiao@qust.edu.cn (K. Jiao).
[1] These authors contributed equally to this study.

0956-5663/$ – see front matter © 2010 Elsevier B.V. All rights reserved.
doi:10.1016/j.bios.2010.11.045

erties of the bulk SPAN, but also have other advantages, such as large specific surface area and excellent electron-transfer ability (Wan, 2008; Shiddiky et al., 2007). NanoSPAN can serve as an attractive alternative of traditional PAN to prepare novel Au micro-/nanostructures/conducting polymer composites in biosensing and biocatalyzing applications.

Generally, the Au micro-/nanostructures/conducting polymer composites are prepared via reduction of $AuCl_4^-$ ions on the conducting polymer modified electrodes (Hatchett and Josowicz, 2008). The prevalent reduction approaches include chemical reduction, hydrogen reduction, polymer matrix reduction and electrochemical reduction etc. (Palmero et al., 2009; Guo and Hu, 2009; Zhang et al., 2009b; Lu et al., 2007). The fabrication methods play a key role in controlling of the morphologies, sizes of Au micro-/nanostructures, which can further affect the electrochemical characteristics of the Au micro-/nanostructures (Lu et al., 2007; Wang et al., 2008). Among the above reduction approaches, electrochemical deposition methods have become popular recently because of their simplicity, low cost and advantages in controlling the purity, particle size and composition of the resulting composite (Zhang et al., 2008).

Herein, a three-step electrodeposition strategy was adopted to fabricate Au microspheres on nanoSPAN coated glassy carbon electrode (Au/nanoSPAN/GCE). The three-step electrodeposition strategy has been reported for the fabrication of polyaniline nanomaterials (Liang et al., 2002; Zhang et al., 2006). To the best of our knowledge, there has been rare report on employing this method for metal deposition up to now. In our system, well hierarchical and homogeneously dispersed flower-like Au microspheres (HHFAu) were obtained in a low $HAuCl_4$ concentration (5.0 mM), which is much lower than previously reported $HAuCl_4$ concentration (24.3 mM, Guo et al., 2007). This highly conductive HHFAu/nanoSPAN membrane was applied to the sensitive impedance detection of the DNA specific sequences of the transgenic genes (the cauliflower mosaic virus 35S gene) in the genetically modified crops.

2. Experimental

2.1. Apparatus and reagents

A CHI 660C electrochemical workstation (Shanghai CH Instrument Company, Shanghai, China) was used for the electrochemical deposition and the electrochemical measurements. A conventional three-electrode system was used with a bare GCE (diameter = 2 mm) or modified GCE as working electrode, a saturated calomel electrode (SCE) as reference electrode and a platinum wire as auxiliary electrode. Scanning electron microscopy (SEM) was carried out using a JSM-5900 microscope (JEOL, Tokyo, Japan). $HAuCl_4{\cdot}4H_2O$ was purchased from Sigma (St. Louis, MO, USA). All of the chemicals used were of analytical grade. Solutions were prepared with aquapro ultrapure water (Ever Young Enterprises Development Co. Ltd., Chongqing, China). The preparations of nanoSPAN see Section 1 of the Supplementary materials.

The cauliflower mosaic virus 35S gene (CaMV35S gene) sequences were synthesized by Beijing SBS Gene Technology Co. Ltd. Their base sequences were as described by Hu (Hu et al., 2010).

All oligonucleotides stock solutions of 18-base oligomers (1.0×10^{-5} M) were prepared with Tris–HCl solution (5.0 mM Tris–HCl, 50.0 mM NaCl, pH 7.0), and stored at 4 °C. More diluted solutions were obtained via diluting aliquot of the stock solution with ultrapure water prior to use. The hybridization solution was diluted with 2× SSC (pH 7.0), which consists of 0.30 M NaCl and 0.030 M sodium citrate tribasic dihydrate ($C_6H_5Na_3O_7{\cdot}2H_2O$).

2.2. Preparation of the Au/nanoSPAN/GCE and Au/GCE

The GCE was carefully polished sequentially with 1, 0.3, and 0.05 μm α-Al_2O_3 pastes on a soft polishing cloth. After being rinsed with ultrapure water, the electrode was cleaned in an ultrasonic bath in water and then 95% ethanol, for 3 min each.

5 μL of 2.0 g/L nanoSPAN suspension (dispersed in ultrapure water) was dripped on the fresh surface of GCE and air-dried naturally to obtain nanoSPAN/GCE. Then, the nanoSPAN/GCE was immersed in a 0.25 M H_2SO_4 solution containing 5.0 mM $HAuCl_4$ for the three-step electrodeposition, which was carried out with three different current densities for fixed periods under the N_2 atmosphere, respectively, 0.06 mA/cm^2 for 0.5 h, 0.03 mA/cm^2 for 2 h and then 0.015 mA/cm^2 for 2 h in turn. After electrodeposition, the obtained electrode was denoted as HHFAu/nanoSPAN/GCE. The one-step (0.06 mA/cm^2 for 0.5 h) and two-step (0.06 mA/cm^2 for 0.5 h and 0.03 mA/cm^2 for 2 h) electrodepositions were also conducted for comparing with the three-step electrodeposition. The fabrication of Au microspheres under other concentrations of $HAuCl_4$ solutions by the three-step electrodeposition was carried out with the same steps as above.

In order to investigate the effect of different current densities, the control experiments were carried out. Three kinds of Au/nanoSPAN/GCEs were respectively fabricated under three different current densities: grown at 0.06 mA/cm^2 for 4.5 h (0.5 h + 2 h + 2 h); grown at 0.03 mA/cm^2 for 4.5 h (0.5 h + 2 h + 2 h); grown at 0.015 mA/cm^2 for 4.5 h (0.5 h + 2 h + 2 h) in a 0.25 M H_2SO_4 solution containing 5.0 mM $HAuCl_4$.

Au/GCE was prepared under the same procedure as illustrated in HHFAu/nanoSPAN/GCE preparation just without nanoSPAN existing.

2.3. Probe DNA immobilization and hybridization

See Section 2 of the Supplementary materials.

2.4. Electrochemical measurements

The cyclic voltammetry (CV) and electrochemical impedance spectroscopic (EIS) measurements were performed with a CHI 660C electrochemical workstation. Cyclic voltammograms were recorded in a 0.1 M KCl solution containing 20.0 mM $K_3[Fe(CN)_6]$ and 20.0 mM $K_4[Fe(CN)_6]$ (1:1) between +0.6 V and −0.2 V at a scan rate of 0.1 V/s. For the EIS measurements, the AC voltage amplitude was +0.005 V, the voltage frequencies ranged from 10^5 Hz to 1 Hz and the applied potential was +0.172 V vs. SCE. The above solution in CV measurements was also used as the supporting electrolyte solution for the EIS experiments.

3. Results and discussion

3.1. Characterization of nanoSPAN function

Au microspheres were synthesized on the bare GCE and the nanoSPAN/GCE, respectively, by the three-step electrodeposition in 5.0 mM $HAuCl_4$ solution. (*Note:* for comparison, the morphologies of the bare GCE and nanoSPAN/GCE were shown in the Section 3 of the Supplementary materials, Fig. S1.) After the electrodeposition, the colour of the bare GCE and the nanoSPAN/GCE surfaces both changed to shining gold, indicating the successful deposition of Au. The SEM images of the resulted modified electrodes are shown in Fig. 1. Low-magnification images (Fig. 1A and 1B) indicate that the as-prepared products both consist of a large quantity of Au microspheres with the diameter about 5 μm. However, the Au microspheres obtained on the nanoSPAN/GCE surface (Fig. 1B) present higher density and more homogeneously dis-

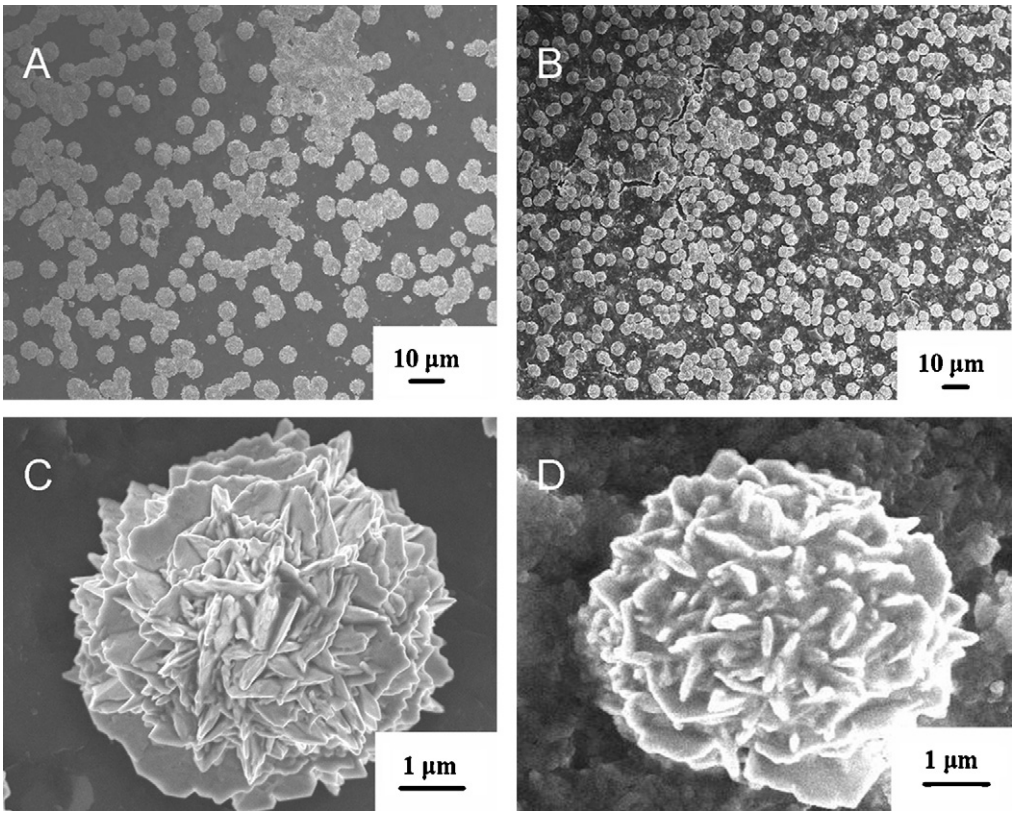

Fig. 1. SEM images of the Au/GCE and HHFAu/nanoSPAN/GCE fabricated by the three-step electrodeposition at different magnifications in 5.0 mM $HAuCl_4$ solution: Au/GCE (A) and HHFAu/nanoSPAN/GCE (B) at low-magnification; Au/GCE (C) and HHFAu/nanoSPAN/GCE (D) at high-magnification.

tribution than those on the bare GCE surface in Fig. 1A. This is probably attributed to the existence of nanoSPAN, which acts as a matrix to support and disperse the Au microspheres and effectively prevent agglomeration of them (Fu et al., 2009). Meanwhile, the sulfonic acid groups and the imine units in nanoSPAN could act as the nuclei for the reduction of Au^{3+} (Reddy et al., 2006), which are beneficial to Au deposition and induce a high density of Au microspheres. High-magnification images (Fig. 1C and D) reveal that these two kinds of Au microspheres both exhibited flower-like structures with flaky outer morphologies. It can be estimated that the nanoscaled flakes (nanoflakes) are of about 100 nm in thickness. The above result indicates that the Au microspheres fabricated by the three-step electrodeposition on these two substrates are similar in morphologies. However, the Au microspheres, which obtained on the nanoSPAN modified electrode, adhered more firmly than the Au microspheres on the bare electrode throughout the processes of electrodeposition and sample washing. The good stability of Au microspheres on nanoSPAN modified electrode is helpful to get a subsequently stable electrochemical signal. This may be attributed to the following two reasons: (1) the nanoSPAN membrane on the electrode surface is very stable. The stability of the nanoSPAN modified electrode was tested in 0.1 M H_2SO_4 solution. Only 7.38% decrease of reduction currents from 1st to 20th cycle at the scan rate of 0.05 V/s was observed (shown in Fig. S2); (2) the presence of the sulfonic acid groups and the imine units in the matrix structure of nanoSPAN could enhance the connection between Au microspheres and the GCE. In short, the well hierarchical and homogeneously dispersed flower-like Au microspheres (HHFAu), which were obtained by the three-step electrodeposition method on the nanoSPAN/GCE in 5.0 mM $HAuCl_4$ solution, have higher density, more homogeneously dispersion and better stability than the Au microspheres directly electrodeposited on the bare GCE under the same conditions.

3.2. Electrochemical activity of HHFAu/nanoSPAN/GCE

CVs of the bare GCE, nanoSPAN/GCE, Au/GCE and HHFAu/nanoSPAN/GCE recorded in 0.1 M KCl containing 20.0 mM $[Fe(CN)_6]^{3-/4-}$ are shown in Fig. 2. The detailed voltammetric parameters of the CVs and the microscopic electroactive areas of the electrodes are shown in the Section 5 of the Supplementary materials, Table S1. As can be seen, compared with the bare GCE (curve a), nanoSPAN/GCE (curve b) and Au/GCE (curve c) both exhibit larger current signals. The improved current responses on the nanoSPAN/GCE and the Au/GCE may be attributed to the larger electroactive surface areas and better electron-transfer ability of these modified electrodes, which could accelerate the electron transfer between $[Fe(CN)_6]^{3-/4-}$ and the GCE. After HHFAu being electrodeposited on the nanoSPAN/GCE (curve d), the redox peak currents of $[Fe(CN)_6]^{3-/4-}$ further increased compared with those

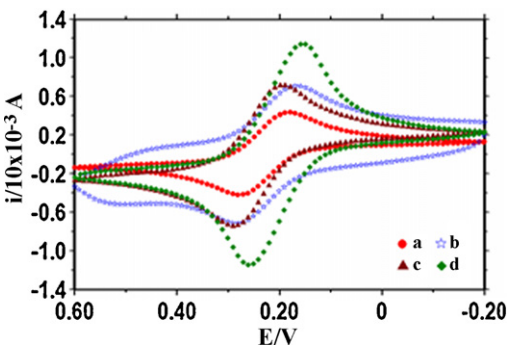

Fig. 2. CVs of 0.1 M KCl containing 20.0 mM $[Fe(CN)_6]^{3-/4-}$ (1:1) recorded at the bare GCE (a), nanoSPAN/GCE (b), Au/GCE (c) and HHFAu/nanoSPAN/GCE (d). Scan rate: 0.1 V/s.

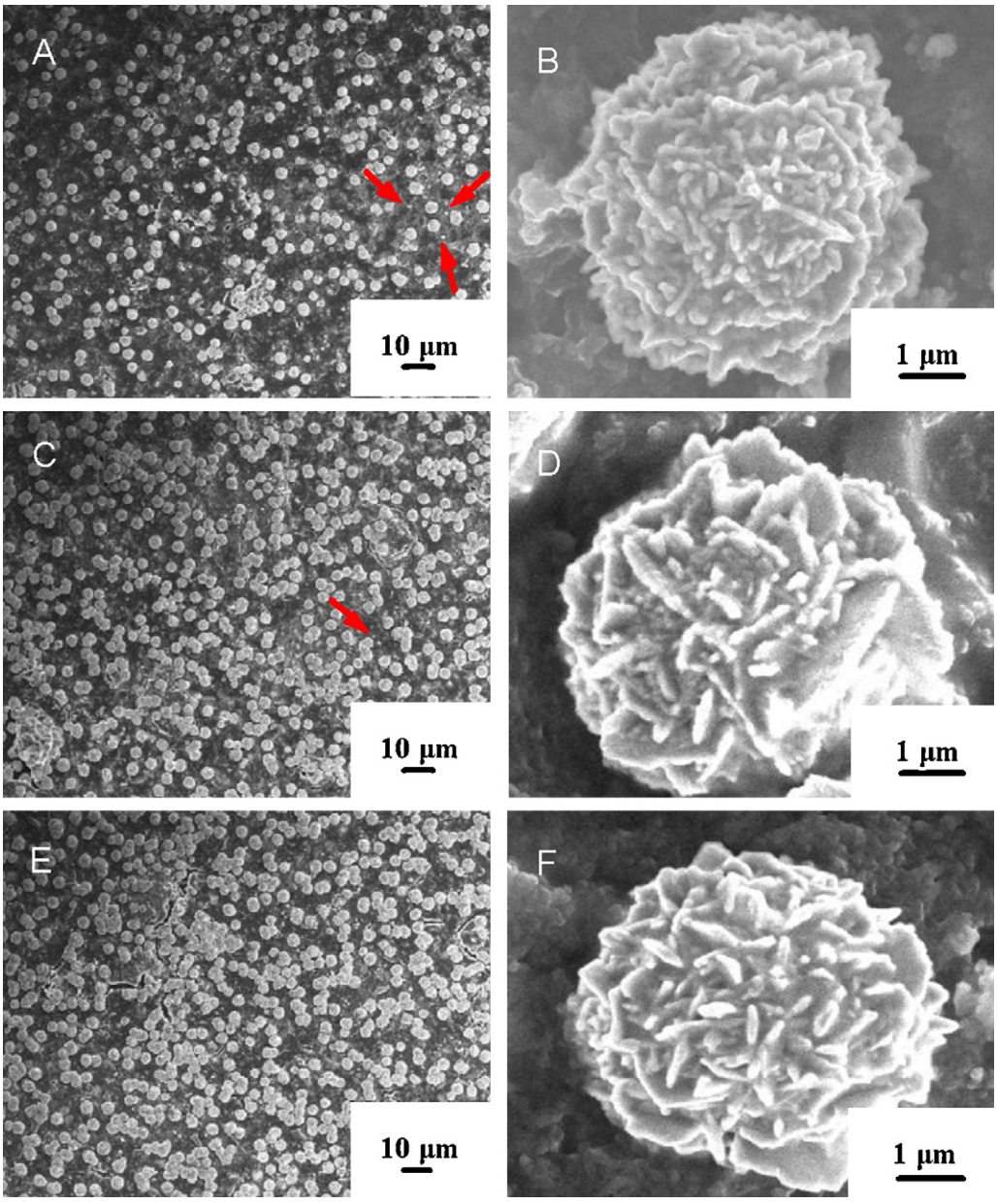

Fig. 3. SEM images of the Au/nanoSPAN/GCEs: fabricated by the one-step electrodeposition (A); two-step electrodeposition (C) and three-step electrodeposition (E). (B), (D) and (F) were the magnified SEM micrographs of (A), (C) and (E), respectively. The concentration of $HAuCl_4$ was 5.0 mM.

of curves a, b and c. The reason may be discussed as two aspects: firstly, the synergistic amplification effect of good conductive properties of the nanoSPAN and Au microspheres accelerates the electron transfer of $[Fe(CN)_6]^{3-/4-}$ on the HHFAu/nanoSPAN membrane; secondly, the better dispersion and higher density of HHFAu on the nanoSPAN modified electrode than the Au microspheres on the GCE, enlarge the microscopic electroactive area significantly (see Section 5 of the Supplementary materials, Table S1) and ensure more efficient charge transport of $[Fe(CN)_6]^{3-/4-}$.

3.3. Effect of the deposition steps on the characters of the Au/nanoSPAN/GCE (discussion for the possible nucleation and growth mechanism of HHFAu)

In order to further study the nucleation and growth process of HHFAu on the nanoSPAN/GCE, the SEM images of the Au/nanoSPAN/GCEs obtained at different deposition steps were shown in Fig. 3. Fig. 3A is the low-magnification image of Au/nanoSPAN composite fabricated by the one-step electrodeposition. It can be seen that the fabricated Au/nanoSPAN/GCE consisted of nanoparticles and microspheres (the Au nanoparticles being typically pointed by red arrows in Fig. 3A and C). These inhomogeneous Au particles locate sparsely on the nanoSPAN/GCE surface with the diameter ranges from several nanometers to approximately 5 μm. The number and the density of the Au microspheres increased after the two-step electrodeposition (Fig. 3C). At the same time, the number and the density of the Au nanoparticles decreased. Compared with the one-step electrodeposition and two-step electrodeposition, the Au microspheres fabricated by the three-step electrodeposition present the largest number and the most homogeneous size dispersion (with a uniform diameter about 5 μm). According to the literatures (Liang et al., 2002; Zhang et al., 2006), the large current density in the first deposition step was mainly applied to create the nucleation sites on the substrate, and the following two reduced current densities were used for the continued nucleation and growth. Hence, it can be estimated that the

nucleation sites were mainly produced in the first deposition step with the large current density. Along with time increasing, some Au nuclei on the substrate underwent crystal growth to small Au nanoparticles or further grew to microspheres. The Au nanoparticles (formed in the first deposition step) and new nuclei (formed in the following deposition steps), can be used as new nucleation sites to grow to extended microspheres accompanying the following second and third deposition steps with lower current densities (0.03 mA/cm^2 and 0.015 mA/cm^2). That is to say, the nucleation mainly took place in the first deposition step and the continued nucleation and growth of the individual Au particle were performed in the second and third deposition steps. However, the nucleation rate of these two steps was much lower than that of the first deposition step. Therefore, after the three-step electrodeposition, the obtained Au microspheres have the highest density and the most uniform size dispersion and Au nanoparticles seem nearly disappeared.

Fig. 3B and D shows the high-magnification SEM images of Au microspheres which were obtained from the one-step and two-step electrodeposition, respectively. As shown in Fig. 3B, the Au microsphere also presents a flower-like structure, but displays an outer morphology consisted of nanoscaled spikes (nanospikes) and nanoflakes, which was different from HHFAu fabricated by the three-step electrodeposition. The nanospikes and nanoflakes are the refined structures of an individual Au microsphere. It seems as if big nanoflakes stacked layer upon layer composed the bottom of the flower-like Au microsphere, and nanospikes and small nanoflakes built up its top. Then, with the increase of deposition steps, the nanospikes gradually grew to the nanoflakes (Fig. 3D). After the three-step electrodeposition, the obtained HHFAu showed flaky outer morphologies without nanospikes nearly (Fig. 3F). It is worth noticing that the growth trend of the nanospikes to nanoflakes in an individual Au microsphere is “bottom to top” and “outside to inside”. It is attributed to that the edges and corners of the nuclei grew faster than its other regions and ahead grew to gold nanoflakes (Li and Shi, 2005). According to the literature (Guo et al., 2007), the small nanoparticles which were deposited on the modified electrode at the beginning of the electrodeposition could act as nanoelectrode ensembles, and a diffusion shielding effect between the nanoelectrodes would be produced when the distance between nanoelectrodes was close. The diffusion shielding effect led to an inhomogeneous distribution of $AuCl_4^-$ around the small gold nanoparticle surfaces in subsequent electrochemical reactions, which is an important factor for the fabrication of flower-like Au microspheres. The transformation from nanospikes to nanoflakes in the three-step electrodeposition process may be related to the changes of the current densities, because the current density has important effect on crystal orientation of the electrodeposited metal (Nakano et al., 2002). When other conditions keep no change, adjusting of the current density will lead to a preferred orientation of the crystal growth, which will result in a faster growth along a certain specific orientation. The diffusion shielding effect together with the preferred crystal orientation played important roles in the formation of HHFAu.

The voltage–time curve of the first deposition step (Supplementary materials, Fig. S3) and the control experiment results indicated by SEM (Supplementary materials, Fig. S4) and XRD (Supplementary materials, Fig. S5) could also be helpful to illustrate the above mechanism.

From the voltage–time curve of the first deposition step (Fig. S3), a sharp decrease of voltage appears during the initial few seconds of the electrodeposition, which corresponds to the process of double-layer charging. Accompanying with the electrodeposition going on, the voltage increased until reached a stabilization state due to the formation of nucleation sites and the free growth of independent nuclei for deposition (Ye et al., 2008).

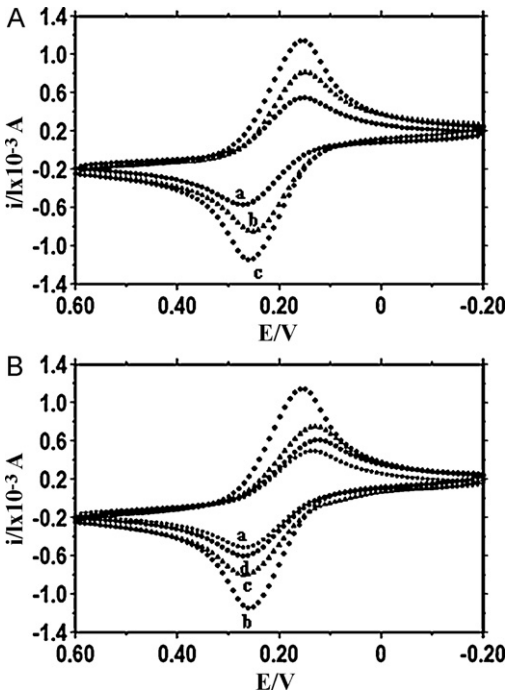

Fig. 4. (A) CVs of 0.1 M KCl containing 20.0 mM $[Fe(CN)_6]^{3-/4-}$ (1:1) recorded at Au/nanoSPAN/GCEs fabricated by the one-step (a); two-step (b) and three-step (c) electrodeposition, respectively. The concentration of $HAuCl_4$ is 5.0 mM. (B) CVs of 0.1 M KCl containing 20.0 mM $[Fe(CN)_6]^{3-/4-}$ (1:1) recorded at Au/nanoSPAN/GCEs fabricated by the three-step electrodeposition in 1.0 mM (a); 5.0 mM (b); 10.0 mM (c) and 20.0 mM (d) $HAuCl_4$ solutions. Scan rate: 0.1 V/s.

The control experiment results shown by SEM (Fig. S4) and XRD (Fig. S5) indicated that the nucleation mainly took place in the first deposition step and the continued nucleation and growth of the individual Au microsphere were performed in the second and third deposition steps, but the nucleation rate of these two steps was much lower than that of the first deposition step. Moreover, the preferred crystal orientation was different among the one-step, two-step and three-step electrodeposition. These results are all consistent with the growth mechanism of HHFAu illustrated above.

3.4. Optimization of other electrodeposition conditions

The deposition conditions have significant effect on the morphologies and the electrochemical behaviors of the resulted metal products. The influence of the deposition steps on the morphologies of the as-prepared Au has been discussed in Fig. 3. Not only the deposition steps but also the $HAuCl_4$ concentration has influence on the morphologies of the resulted Au microspheres, which is shown in the Section 9 of the Supplementary materials, Figs. S6 and S7. The results demonstrate that the morphology of Au can also be easily controlled by changing the $HAuCl_4$ concentration.

The effect of the deposition steps and $HAuCl_4$ concentration on the electrochemical behaviors of the resulted Au/nanoSPAN/GCE has also been studied, as shown in Fig. 4. Fig. 4A shows the CVs of 0.1 M KCl containing 20.0 mM $[Fe(CN)_6]^{3-/4-}$ recorded at Au/nanoSPAN/GCEs prepared in 5.0 mM $HAuCl_4$ by the one-step (curve a), two-step (curve b) and three-step (curve c) electrodeposition, respectively. The biggest peak current appeared at HHFAu/nanoSPAN/GCE which was fabricated by the three-step electrodeposition. It was attributed to the highest density of the Au microspheres and the largest electroactive surface area of the HHFAu/nanoSPAN/GCE.

CVs recorded for Au/nanoSPAN/GCEs electrodeposited in different concentrations of $HAuCl_4$ solutions through the three-step

Table 1
Comparison of the proposed biosensor with the previously reported DNA sensors based on Au nanocomposites with EIS measurements.

Electrode	Detection range (M)	Detection range (M)	References
Au-Bd2MPTS	1.0×10^{-8} to 1.0×10^{-5}	5.0×10^{-9}	Fu et al. (2005)
Au/PDC/GCE	1.0×10^{-10} to 1.0×10^{-5}	2.4×10^{-11}	Yang et al. (2007)
Au/nanoPAN/GCE	1.0×10^{-12} to 1.0×10^{-6}	3.1×10^{-13}	Feng et al. (2008)
HHFAu/nanoSPAN/GCE	1.0×10^{-13} to 1.0×10^{-6}	1.9×10^{-14}	This work

electrodeposition are shown in Fig. 4B. Accompanying with the increase of the $HAuCl_4$ concentration from 1.0 mM to 5.0 mM, the obtained HHFAu/nanoSPAN/GCE presents an obviously elevated activity for $[Fe(CN)_6]^{3-/4-}$ redox behavior. However, further increase in the $HAuCl_4$ concentration induces a decrease tend of CV signals of $[Fe(CN)_6]^{3-/4-}$. These results indicate that the HHFAu/nanoSPAN/GCE electrodeposited in 5.0 mM $HAuCl_4$ solution by the three-step electrodeposition shows the highest electrochemical activity towards the electron transfer of the redox probe ($[Fe(CN)_6]^{3-/4-}$).

3.5. DNA biosensor based on HHFAu/nanoSPAN/GCE

Since the HHFAu/nanoSPAN/GCE fabricated by the three-step electrodeposition in 5.0 mM $HAuCl_4$ exhibits large electroactive surface area, excellent electron transfer ability and good biocompatibility, it can serve as a DNA biosensing platform for DNA hybridization detection. The DNA immobilization and hybridization were verified by EIS using 20.0 mM $[Fe(CN)_6]^{3-/4-}$ as an electroactive probe. EIS analysis was employed to study the impedance changes of the electrode surface and provide further evidence for interface assembly on the electrode including immobilization and hybridization reaction of DNA (Daniels and Pourmand, 2007). The Bode plots of the EIS measurement are shown in Fig. 5A. The impedance value ($\log Z$) at 10^4 Hz in the corresponding Bode plot was selected for comparison. Curve a is the Bode plot of the HHFAu/nanoSPAN/GCE. When the probe DNA (pDNA) was bound onto the modified electrode surface, the $\log Z$ increased (curve b). The increment of impedance indicates that the pDNA was successfully immobilized on the electrode surface. The reason was that the negatively charged phosphate backbone of the pDNA prevents $[Fe(CN)_6]^{3-/4-}$ from reaching the electrode surface and leads to a much larger impedance value (Tian et al., 2004; Yang et al., 2009). A maximal impedance value is observed after hybridization of the pDNA with its complementary sequence DNA (cDNA) (curve c). This may be attributed to more negative charges and thicker DNA modified layer of the dsDNA/HHFAu/nanoSPAN/GCE. This result demonstrates that the HHFAu/nanoSPAN/GCE could be used for electrochemical DNA hybridization detection. The impedance value obtained from the hybridization of the probe electrode with double-base mismatched DNA (curve d) decreases compared with that of the curve c. When the pDNA hybridized with non-complementary sequence DNA (ncDNA) (curve e), little impedance value change is detected compared with that of curve b. This fact indicates that the pDNA modified electrode could also distinguish the mismatched DNA and ncDNA. The above results show the good selectivity of this biosensor.

The probe electrode was used to detect the CaMV35S gene target sequences from transgenically modified plants and the Bode plots were obtained after hybridization with different concentrations of the complementary target sequences, as shown in Fig. 5B. The difference (namely $\Delta \log Z$) between the $\log Z$ value of the probe-captured electrode and that after hybridization with cDNA at 10^4 Hz was adopted as the measurement signal. The $\Delta \log Z$ value is linear with the logarithm of the CaMV35S gene target sequence concentrations (Supplementary materials, Fig. S8, the calibration curve was obtained by 6 parallel measurements

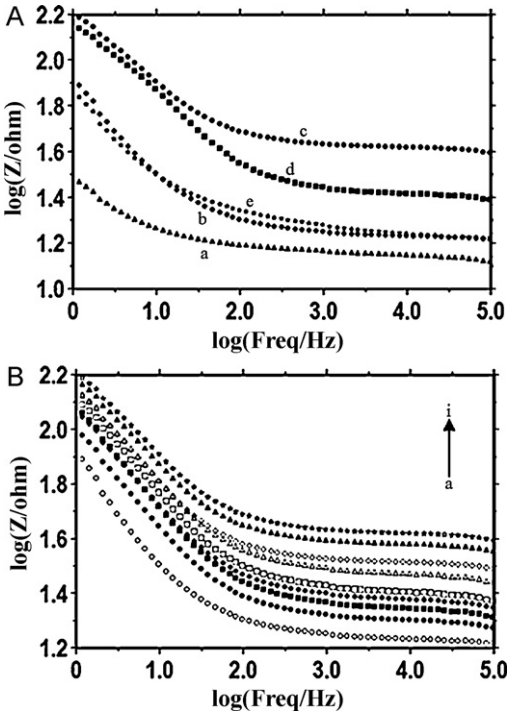

Fig. 5. (A) Bode plots recorded at the HHFAu/nanoSPAN/GCE (a); ssDNA/HHFAu/nanoSPAN/GCE (b); dsDNA/HHFAu/nanoSPAN/GCE (hybridized with cDNA) (c); the probe electrode hybridized with double-base mismatched DNA (d) and the probe electrode hybridized with ncDNA (e) in 0.1 M KCl containing 20.0 mM $[Fe(CN)_6]^{3-/4-}$ (1:1); (B) Bode plots recorded at the ssDNA/HHFAu/nanoSPAN/GCE (a) and after hybridization reaction with its complementary CaMV35S gene sequences of different concentrations: 1.0×10^{-13} M (b); 1.0×10^{-12} M (c); 1.0×10^{-11} M (d); 1.0×10^{-10} M (e); 1.0×10^{-9} M (f); 1.0×10^{-8} M (g); 1.0×10^{-7} M (h) and 1.0×10^{-6} M (i). The AC voltage amplitude was 0.005 V.

at each concentration with regeneration sensor). The dynamic detection range for the sequence-specific DNA of CaMV35S gene is from 1.0×10^{-13} M to 1.0×10^{-6} M with the regression equation $\Delta \log Z = 0.0116 \log C + 0.1520$ and the regression coefficient (γ) 0.9985. The detection limit of this impedance detection assay is 1.9×10^{-14} M using 3σ (where σ was the relative standard deviation of 11 parallel measurements of the blank solution).

The DNA biosensor had good stability, high reproducibility and fine regeneration ability (see Section 11 of the Supplementary materials).

The comparison of the proposed biosensor with other biosensors based on Au nanocomposites with EIS measurements was listed in Table 1. It can be seen that this DNA sensor had broader dynamic detection range and lower detection limit for the target DNA assay.

4. Conclusions

A novel three-step electrodeposition for the preparation of well hierarchical and homogeneously dispersed flower-like Au microspheres from $HAuCl_4$ electrolytes was demonstrated in this paper. The relationship between electrodeposition condi-

tions (such as deposition step and $HAuCl_4$ concentration) and the resulted Au morphologies was investigated in detail. The nucleation mainly takes place in the first deposition step and the continued nucleation and growth of the individual Au microsphere are performed in the second and third deposition steps. The growth trend of the nanospikes to nanoflakes in an individual Au microsphere is "bottom to top" and "outside to inside". The resulting HHFAu/nanoSPAN/GCE brings new capabilities for electrochemical devices by utilizing synergistic action of HHFAu and nanoSPAN to facilitate electron-transfer process and improve electroactive surface area of electrode. Due to the unique chemical and structural properties of HHFAu/nanoSPAN and the high sensitivity of EIS technique, a novel impedance biosensing platform for DNA hybridization recognition was successfully developed, which owns high sensitivity, good stability, fine reproducibility and nice regeneration ability. The fragment related to CaMV35S gene is satisfactorily detected with a low detection limit (1.9×10^{-14} M).

Acknowledgments

This work was supported by the National Natural Science Foundation of China (No. 20635020, No. 20805025 and No. 20975057), the Foundation of Qingdao City (No. 09-1-3-25-jch) and the Doctoral Fund of QUST (0022278).

Appendix A. Supplementary data

Supplementary data associated with this article can be found, in the online version, at doi:10.1016/j.bios.2010.11.045.

References

Crespilhoa, F.N., Iost, R.M., Travainc, S.A., Oliveira Jr., O.N., Zucolottob, V., 2009. Biosens. Bioelectron. 24, 3073–3077.
Daniels, J.S., Pourmand, N., 2007. Electroanalysis 19, 1239–1257.
Feng, Y.Y., Yang, T., Zhang, W., Jiang, C., Jiao, K., 2008. Anal. Chim. Acta 616, 144–151.
Fu, Y.C., Li, P.H., Xie, Q.J., Xu, X.H., Lei, L.H., Chen, C., Zou, C., Deng, W.F., Yao, S.Z., 2009. Adv. Funct. Mater. 19, 1784–1791.
Fu, Y.Z., Yuan, R., Xu, L., Chai, Y.Q., Zhong, X., Tang, D.P., 2005. Biochem. Eng. J. 23, 37–44.
Gao, Y., Chen, C.A., Gau, H.M., Bailey, J.A., Akhadov, E., Williams, D., Wang, H.L., 2008. Chem. Mater. 20, 2839–2844.
Granot, E., Katz, E., Basnar, B., Willner, I., 2005. Chem. Mater. 17, 4600–4609.
Guo, S.J., Wang, L., Wang, E.K., 2007. Chem. Commun., 3163–3165.
Guo, S.J., Dong, S.J., Wang, E.K., 2009. Small 5, 1869–1876.
Guo, X.H., Hu, N.F., 2009. J. Phys. Chem. C 113, 9831–9837.
Hatchett, D., Josowicz, M., 2008. Chem. Rev. 108, 746–769.
Hu, Y.W., Yang, T., Wang, X.X., Jiao, K., 2010. Chem. Eur. J. 16, 1992–1999.
Lee, D., Donkers, Ro.L., Wang, G., Harper, A.S., Murray, R.W., 2004. J. Am. Chem. Soc. 126, 6193–6199.
Li, Y., Shi, G.Q., 2005. J. Phys. Chem. B 109, 23787–23793.
Liang, L., Liu, J., Windisch Jr., C.F., Exarhos, G.J., Lin, Y.H., 2002. Angew. Chem. Int. Ed. 41, 3665–3668.
Lu, G.W., Li, C., Shi, G.Q., 2007. Chem. Mater. 19, 3433–3440.
Nakano, H., Nakahara, K., Kawano, S., Oue, S., Akiyama, T., Fukushima, H., 2002. J. Appl. Electrochem. 32, 43–48.
Njagi, J., Andreescu, S., 2007. Biosens. Bioelectron. 23, 168–175.
Palmero, S., Colina, A., Munoz, E., Heras, A., Ruiz, V., Palacios, J.L., 2009. Electrochem. Commun. 11, 122–125.
Pringle, J.M., Jensen, O.W., Lynam, C., Wallace, G.G., Forsyth, M., MacFarlane, D.R., 2008. Adv. Funct. Mater. 18, 2031–2040.
Rahman, M.A., Noh, H.B., Shim, Y.B., 2008. Anal. Chem. 80, 8020–8027.
Reddy, K.R., Lee, K.P., Gopalan, A.I., Kim, M.S., Showkat, A., Nho, Y.C., 2006. J. Polym. Sci. Pol. Chem. 44, 3355–3364.
Shiddiky, M.J.A., Rahman, M.A., Shim, Y.B., 2007. Anal. Chem. 79, 6886–6890.
Singh, K., Rahman, M.A., Son, J.I., Kim, K.C., Shim, Y.B., 2008. Biosens. Bioelectron. 23, 1595–1601.
Subramanian, V., Wolf, E.E., Kamat, P.V., 2004. J. Am. Chem. Soc. 126, 4943–4950.
Tarver, J., Yoo, J.E., Dennes, T.J., Schwartz, J., Loo, Y.L., 2009. Chem. Mater. 21, 280–286.
Tian, S.J., Liu, J.Y., Zhu, T., Knoll, W., 2004. Chem. Mater. 16, 4103–4108.
Wan, M.X., 2008. Adv. Mater. 20, 2926–2936.
Wang, S.P., Wu, Z.S., Qu, F.L., Zhang, S.B., Shen, G.L., Yu, R.Q., 2008. Biosens. Bioelectron. 24, 1020–1026.
Yang, J., Yang, T., Feng, Y.Y., Jiao, K., 2007. Anal. Biochem. 365, 24–30.
Yang, T., Zhou, N., Zhang, Y.C., Zhang, W., Jiao, K., Li, G.C., 2009. Biosens. Bioelectron. 24, 2165–2170.
Ye, F., Li, J.J., Wang, T.T., Liu, Y., Wei, H.J., Li, J.L., Wang, X.D., 2008. J. Phys. Chem. C 112, 12894–12898.
Zhang, L., Jiang, X., Niu, L., Dong, S.J., 2006. Biosens. Bioelectron. 21, 1107–1115.
Zhang, H., Xu, J.J., Chen, H.Y., 2008. J. Phys. Chem. C 112, 13886–13892.
Zhang, C.Q., Li, G.C., Peng, H.R., 2009a. Mater. Lett. 63, 592–594.
Zhang, J.J., Gu, M.M., Zheng, T.T., Zhu, J.J., 2009b. Anal. Chem. 81, 6641–6648.
Zhang, W., Yang, T., Li, X., Wang, D.B., Jiao, K., 2009c. Biosens. Bioelectron. 25, 428–434.
Zhao, W.A., Chiuman, W., Lam, J.C.F., McManus, S.A., Chen, W., Cui, Y.G., Pelton, R., Brook, M.A., Li, Y.F., 2008. J. Am. Chem. Soc. 130, 3610–3618.